OPEN ACCESS



Shock Heating of Incident Thermal and Superthermal Populations of Different Ion Species

Michael Gedalin , Vadim Roytershteyn , and Nikolai V. Pogorelov , ^{3,4}

Department of Physics, Ben Gurion University of the Negev, Beer-Sheva, Israel; gedalin@bgu.ac.il

Space Science Institute, Boulder, CO 80301, USA

Department of Space Science, The University of Alabama in Huntsville, AL 35805, USA

Center for Space Plasma and Aeronomic Research, The University of Alabama in Huntsville, AL 35805, USA

Received 2022 October 26; revised 2023 January 6; accepted 2023 January 6; published 2023 March 7

Abstract

Using ion tracing in a model shock front we study heating of thermal (Maxwellian) and superthermal (Vasyliunas—Siscoe) populations of protons, singly charged helium, and alpha particles. It is found that heating of thermal and superthermal populations is different, mainly because of substantially higher ion reflection in the superthermal populations. Accordingly, the temperature increase of initially superthermal populations is substantially higher than that of the thermal ions. Heating per mass decreases with the increase of the mass-to-charge ratio because of the reduced effect of the cross-shock potential and, accordingly, weaker ion reflection. The findings are supported by two-dimensional hybrid simulations.

Unified Astronomy Thesaurus concepts: Shocks (2086); Interplanetary shocks (829); Planetary bow shocks (1246); Heliosphere (711)

1. Introduction

Collisionless shocks are extremely efficient in the conversion of the energy of the directed flow into energy of heated and accelerated particles. In magnetized shocks, the width of the main magnetic field increase (ramp) is substantially smaller than the ion convective gyroradius (Greenstadt et al. 1975; Greensadt et al. 1980; Russell et al. 1982; Mellott & Greenstadt 1984; Newbury et al. 1998; Bale et al. 2003, 2005; Hobara et al. 2010; Krasnoselskikh et al. 2013); for this reason, ion heating is nonadiabatic (Sckopke et al. 1983, 1990). Upon crossing the ramp, ions begin to gyrate around the downstream magnetic field. After gyrophase-mixing further from the transition, this gyration is measured as a velocity spread in the flow frame, i.e., the ion temperature (Gedalin 1997a, 1997b; Pope et al. 2019; Gedalin 2021). In higher-Mach number shocks, $M \gtrsim 3$, ion reflection is significant. Here M is the Alfvénic Mach number (see definitions in Section 2). Reflected ions, upon the second crossing of the shock toward downstream, have higher gyration speeds and may dominate the downstream temperature (Woods 1969, 1971; Leroy et al. 1982; Sckopke et al. 1983; Scudder et al. 1986; Burgess et al. 1989; Sckopke et al. 1990; Bale et al. 2005; Richardson 2010; Zimbardo 2011; Broll et al. 2018). Ion reflection enhances with the increase of the Alfvénic Mach number. Ion reflection depends on the shock angle and the magnetic compression (the latter is not independent of the Mach number, though) and is also sensitive to the ratio of the thermal speed of the incident ions to the shock speed (Gedalin 1996, 2016; Balikhin & Gedalin 2022). Superthermal ions have more chances to be reflected. Thus, presence of a substantial superthermal population may significantly affect the formed downstream distributions and the overall heating of ions at the shock front. Ions with larger mass-to-charge ratio have large gyroradii. They also lose a smaller part of their initial energy to overcome the cross-shock potential. Accordingly, they are

Original content from this work may be used under the terms of the Creative Commons Attribution 4.0 licence. Any further distribution of this work must maintain attribution to the author(s) and the title of the work, journal citation and DOI.

expected to retain a larger fraction of their initial energy and a gyration energy and therefore would be heated more efficiently (Gedalin 2020). The objective of the present paper is to study the differences in the heating of thermal and superthermal populations both for protons and heavier ions. This is done by separate analysis of the downstream distributions produced upon crossing a quasiperpendicular shock by thermal ions and markedly superthermal ions.

2. Model and Method

We analyze downstream ion distributions by tracing ion trajectories in a model shock profile. Since we are interested in understanding the difference between heating of thermal and superthermal populations of protons and heavier ions under the same conditions, in the present paper we limit ourselves with a planar, stationary low-Mach number shock model. In what follows, subscripts u and d denote upstream and downstream, respectively. Let the shock normal be in x-direction and x-z be the coplanarity plane. The chosen magnetic field profile is given by the following expression:

$$B_z = B_u \sin \theta \left(\frac{R-1}{2} + \frac{R+1}{2} \tanh \frac{3x}{D} \right), \tag{1}$$

where B_u is the upstream magnetic field magnitude and θ is the angle between the shock normal and the upstream magnetic field vector. The magnetic compression is

$$\frac{B_d}{B_u} = \sqrt{R^2 \sin^2 \theta + \cos^2 \theta}.$$
 (2)

The shock width is given by the parameter D. The upstream proton gyrofrequency is $\Omega_u = eB_u/m_pc$, and the upstream proton plasma frequency is $\omega_p = \sqrt{4\pi e^2 n_u/m_p}$, where n_u is the upstream proton number density. The ion inertial length is c/ω_p , and the Alfvén speed is $v_A = c\Omega_u/\omega_p$. Let the upstream plasma velocity along the shock normal in the shock frame be V_u , then the Alfvénic Mach number is $M = V_u/v_A$. The

upstream convective proton gyroradius is $\rho_p = V_u/\Omega_u = M(c/\omega_p)$. Accordingly, the following normalization is used:

$$\frac{x}{\rho_n} \to x, \quad \Omega_u t \to t, \quad \frac{\mathbf{v}}{V_u} \to \mathbf{v}, \quad \frac{\mathbf{B}}{B_u} \to \mathbf{B}.$$
 (3)

Ion tracing is performed in the de Hoffman–Teller frame (HT), in which the upstream and downstream plasma velocities are along the upstream and downstream magnetic field vectors, respectively. The motional electric field $E_y = 0$ vanishes identically in HT, like the component E_z . The shape of the cross-shock electric field is chosen as follows:

$$E_x = -K_E \frac{dB_z}{dx},\tag{4}$$

where the coefficient K_E is determined from the cross-shock potential.

$$\phi_{\rm HT} = -\int_{-\infty}^{\infty} E_x dx \tag{5}$$

is one of the model parameters. In the dimensionless form,

$$s_{\rm HT} = e\phi_{\rm HT}/(m_p V_u^2/2).$$
 (6)

The noncoplanar magnetic field shape is chosen in a similar form:

$$B_{y} = K_{B} \frac{dB_{z}}{dx},\tag{7}$$

while

$$\phi_{\rm NIF} - \phi_{\rm HT} = \frac{V_u \tan \theta}{c} \int_{-\infty}^{\infty} B_y dx.$$
 (8)

Here the subscript NIF means normal incidence frame, in which the upstream plasma flow is along the shock normal. The parameter

$$s_{\rm NIF} = e\phi_{\rm NIE}/(m_p V_u^2/2) \tag{9}$$

is the model parameter that determines the coefficient K_B . In the present analysis $s_{\rm NIF}=0.3$, $s_{\rm HT}=0.1$, and $D=(c/\omega_{pp})$. The chosen Mach number is M=2.6. The shock angle is $\theta=70^{\circ}$. The magnetic compression $B_d/B_u=2.25$ is derived from Rankine–Hugoniot relations (Karimabadi et al. 1988) with $\beta_e=\beta_p=8\pi n_u T_u/B_u^2=0.2$ with the downstream anisotropy $p_{\parallel}/p_{\perp}=0.7$. Here T_u is the upstream ion temperature.

The ion tracing is done by numerically solving the equations of motion

$$\frac{d\mathbf{r}}{dt} = \mathbf{v}, \quad \frac{d\mathbf{v}}{dt} = \frac{q}{m} \left(\mathbf{E} + \frac{1}{c} \mathbf{v} \times \mathbf{B} \right) \tag{10}$$

in the fields prescribed by the above model for a specified distribution function of the incident ions. This is equivalent to solving the Vlasov equation for the distribution function, which is time independent and depends only on the coordinate along the shock normal, f = f(v, x):

$$\frac{\partial f}{\partial x} + \frac{q}{m} \left(E + \frac{1}{c} \mathbf{v} \times \mathbf{B} \right) \frac{\partial f}{\partial \mathbf{v}} = 0. \tag{11}$$

Let (v, x) belong to the solution of Equation (10) for the initial conditions (v_0, x_0) . Then the solution of the Vlasov equation is

 $f(\mathbf{v}, x) = f_0(\mathbf{v}_0, x_0)$, where f_0 is the distribution function of the incident ions. Any calculation involving integration over velocities at some position x with the distribution function at this position can be performed using (Gedalin et al. 2015)

$$f(\mathbf{v}, x)d^3\mathbf{v} = f(\mathbf{v}_0, x_0)d^3\mathbf{v}_0 \frac{|\mathbf{v}_{0x}|}{|\mathbf{v}_x|}.$$
 (12)

Using Equation (12), we numerically determine the distribution function assigning each particle the weight $|v_{0x}|$ and catching it in a thin layer of the width Δx as many times as this particle appears there (the staying-time method). The number of counts is $\Delta x/|v_x|\Delta t$, where Δt is time step. In this way the reduced distribution function (see Equation (22) below) is derived. Sufficiently far from the shock transition the parallel and perpendicular velocities in HT do not vary any longer, which allows us to numerically calculate $f(v_{\parallel}, v_{\perp})$, where \parallel and \perp refer to the local magnetic field direction (either upstream or downstream). Backstreaming ions would be seen as $f_u(v_{\parallel}, v_{\perp})$ for $v_{\parallel} < 0$. Within this approach there is no need to treat separately thermal and superthermal particles, and virtually any initial distribution can be analyzed.

3. Downstream Distributions

In what follows we analyze the following populations: a) thermal Maxwellian protons with T_u corresponding to $\beta_p = 0.2$ (PM); b) superthermal Vasyliunas–Siscoe (VS; Vasyliunas & Siscoe 1976) protons (PV); c) thermal Maxwellian singly ionized helium He⁺ (hereafter HM), $m_{\text{He}^+} = 4m_p$, $q_{\text{He}^+} = e$, with T_u corresponding to $\beta_{\text{He}^+} = 0.2$; d) superthermal VS singly ionized helium (HV); e) thermal Maxwellian $\alpha = \text{He}^{++}$ particles (AM), $m_\alpha = 4m_p$, $q_\alpha = 2e$, with T_u corresponding to $\beta_\alpha = 0.2$ and f) superthermal VS α particles (AV).

We start with the Maxwellian distributed protons

$$f(\mathbf{v}) = \frac{n_u}{(2\pi)^{3/2} v_T^3} \exp\left(-\frac{(\mathbf{v} - \mathbf{V})^2}{2v_T^2}\right),\tag{13}$$

where V is the plasma velocity and $v_T/V_u = \sqrt{\beta/2}/M$. This population is assumed to be shock forming, while all others are treated as small additions not affecting the shock profile. Figure 1 shows the comparison of the model magnetic field magnitude (blue curve) with the magnetic field magnitude derived from the pressure balance (red curve). 40,000 protons from the initial Maxwellian distribution (Equation (13)) were traced in the model magnetic and electric fields. In a planar stationary shock, the momentum conservation along the shock normal (pressure balance) reads

$$nm_p V_x^2 + p_{xx} + \frac{B^2}{8\pi} = \text{const},$$
 (14)

where

$$n = \int f(\mathbf{v}, x) d\mathbf{v},\tag{15}$$

$$nV = \int v f(v, x) dv, \tag{16}$$

$$p_{ij} = m \int v_i v_j f(\mathbf{v}, x) d\mathbf{v}. \tag{17}$$

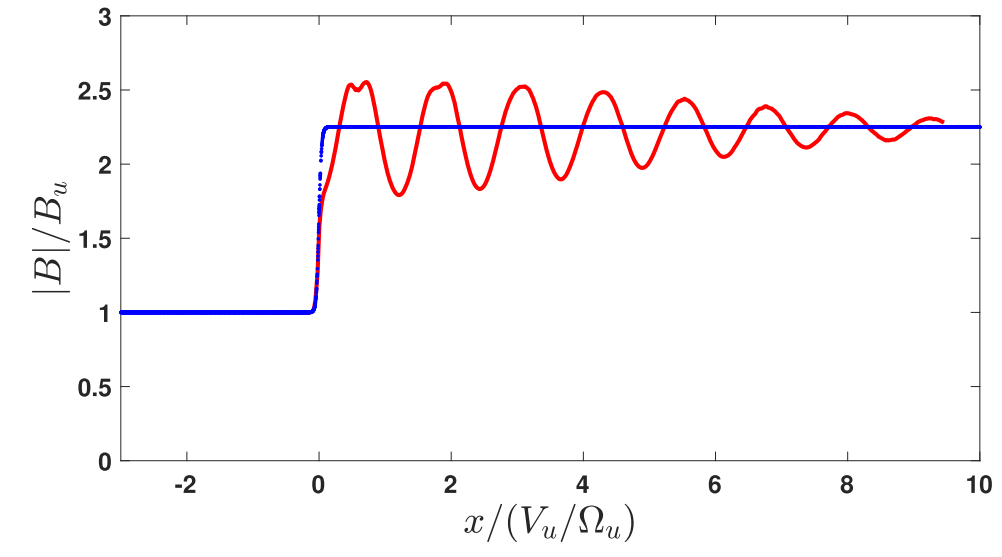


Figure 1. The model magnetic field magnitude (blue) vs. the magnetic field derived from the pressure balance (Equation (14); red).

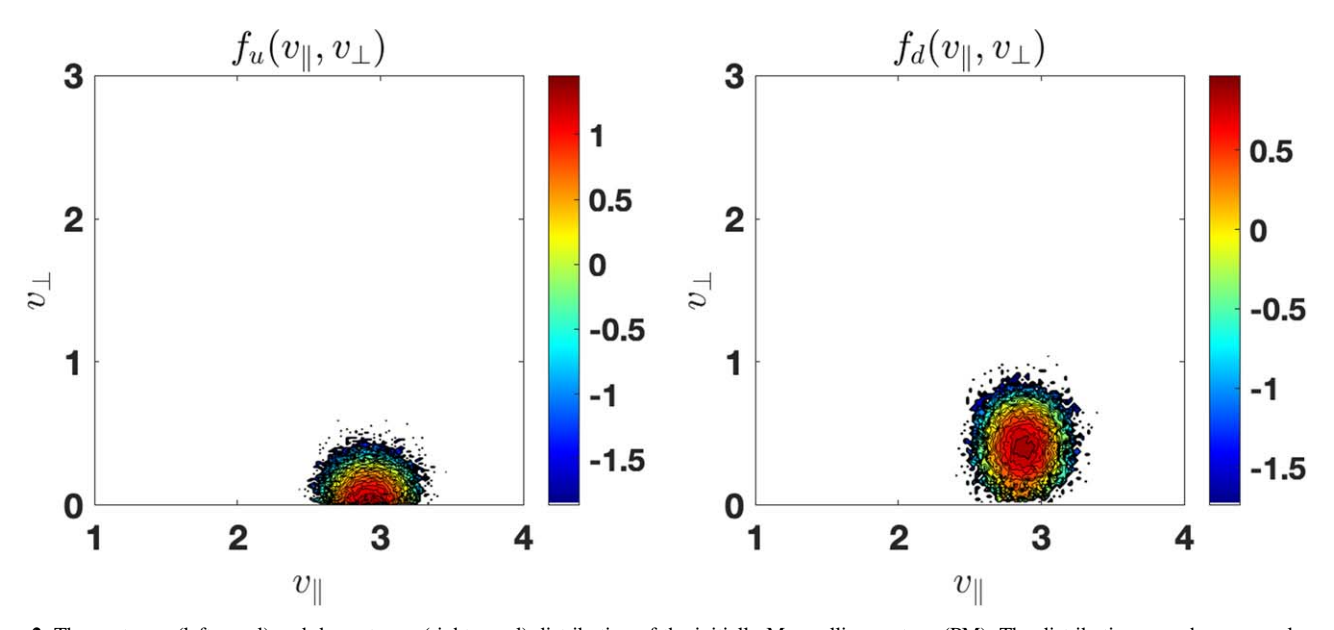


Figure 2. The upstream (left panel) and downstream (right panel) distribution of the initially Maxwellian protons (PM). The distributions are shown on a log scale.

Here $f(\mathbf{v}, x)$ is the velocity distribution function that depends on x only, and i and j = x, y, z. The quantities $nm_pV_r^2$ and p_{xx} are determined numerically from the traced ion distribution. The red curve in Figure 1 is the magnetic field derived from Equation (14). Note that the value $s_{NIF} = 0.3$ is obtained numerically, after several tries, from the requirement that far downstream, the two curves converge. The derived profile shows a weak overshoot and magnetic oscillations that are expected for these chosen Mach numbers and β . Note that the shock is supercritical with ion reflection, which results in a slight deviation of the derived profile from the model profile ahead of the ramp. All these deviations are not significant for the analysis of ion heating. In this comparison, it is assumed that the Maxwellian protons are the main component of the plasma. All other populations are assumed to be small admixtures and are treated as test particles with negligible contribution to the pressure. The comparison of the model

magnetic field and the magnetic field derived from Equation (14) is presented to show the consistency of the chosen model.

Figure 2 shows the upstream (left panel) and downstream (right panel) distribution of the initially Maxwellian protons on the logarithmic scale. Here

$$v_{\parallel} = (\mathbf{v} - \mathbf{V}) \cdot \mathbf{B}/|\mathbf{B}|, \quad v_{\perp} = |(\mathbf{v} - \mathbf{V}) \times \mathbf{B}|/|\mathbf{B}|.$$
 (18)

The downstream distribution $f_d(v)$ is constructed far from the ramp, where the magnetic oscillations already disappear, and the distribution is already gyrotropic. The parallel and perpendicular temperatures are defined as follows:

$$nT_{\parallel} = \int v_{\parallel}^2 f_d(\mathbf{v}) d\mathbf{v} \tag{19}$$

$$nT_{\perp} = \frac{1}{2} \int v_{\perp}^2 f_d(\mathbf{v}) d\mathbf{v}. \tag{20}$$

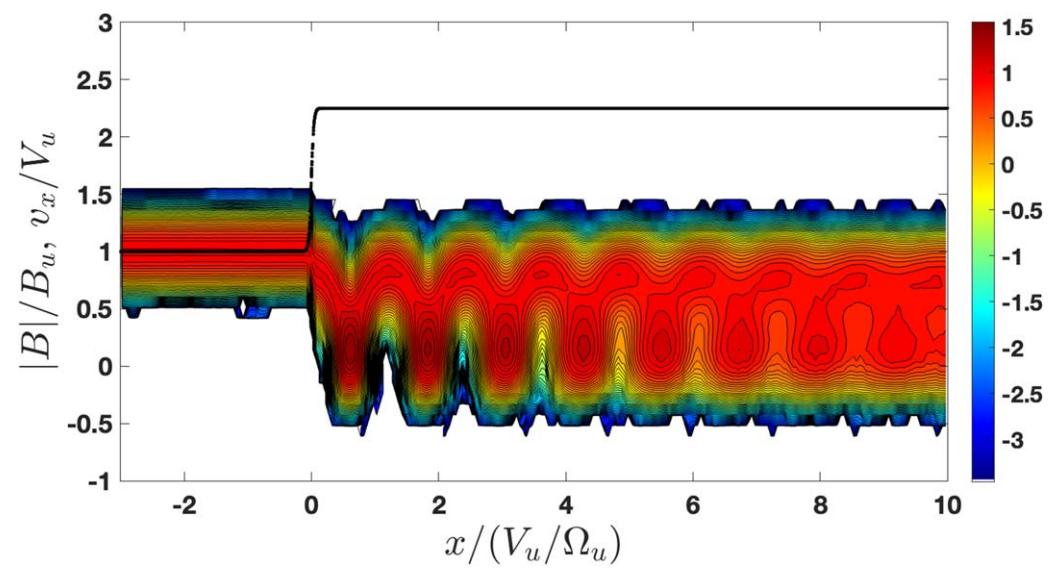


Figure 3. The reduced distribution function (Equation (22)) on a log scale.

For this population,

$$\frac{T_u}{m_p V_u^2} \approx \frac{T_{d,\parallel}}{m_p V_u^2} \approx 0.01, \quad \frac{T_{d,\perp}}{m_p V_u^2} \approx 0.1,$$
(21)

so that the downstream distribution is strongly anisotropic, $T_{d,\perp}/T_{d,\parallel}\approx 10$. Anisotropic heating is typical for magnetized shocks and sometimes is taken into account when using Rankine–Hugoniot relations (Abraham-Shrauner 1967; Lynn 1967; Hudson 1970; Vogl et al. 2001; Génot 2009). Note that these high anisotropies would disappear due to isotropization farther from the shock transition. Here we are interested in what happens at the shock front itself.

Figure 3 shows the reduced distribution function

$$f_r(v_x, x) = \int f(\mathbf{v}, x) dv_y dv_z. \tag{22}$$

The gyrating ion distribution and the kinematic collisionless relaxation are clearly seen.

Roughly speaking, there are two modes of ion reflection (Gedalin 2016). The "electric reflection" occurs when an ion cannot overcome the cross-shock potential so that their $v_x = 0$ at some point inside the ramp. These ions have low velocities along the shock normal at their entry into the ramp. Reflection in this mode is not solely due to the electric field since magnetic deflection also can contribute to the reduction of v_r for appropriate gyrophases. The "magnetic reflection" occurs when an ion crosses the ramp, gyrates in the magnetic field behind the ramp, comes back to it, and crosses it again from the downstream region to the upstream region. These ions come from another part of the tail of the Maxwellian distribution since they should have sufficiently high v_x and appropriate gyrophases at the entry into the ramp. Note that the terms "electric reflection" and "magnetic reflection" are used only for brevity and convenience and do not mean that only electric or magnetic forces are responsible for the ion dynamics in either case. It is always a combined effect. For low magnetic compressions, B_d/B_u and low β magnetic reflection is not efficient. Efficiency of electric reflection depends on the ratio $v_h = v_T / V_u = \sqrt{\beta/2} / M$. The number of ions in the low

velocity tail of the distribution rapidly increases with the increase of v_h . Thus, the efficiency of this reflection mode increases with the increase of the upstream ion temperature and decreases with the increase of the Mach number for a constant cross-shock potential.

Figure 4 shows the upstream (left panel) and downstream (right panel) distribution of the initially vs. distributed protons. The upstream distribution function is

$$f_{VS} = \frac{3n_{VS}}{8\pi u^{3/2}} H(V_u - u),$$

$$u = \sqrt{(v_x - V_u)^2 + v_y^2 + (v_z - V_u \tan \theta)^2},$$
(23)

where H(x) is the step function. In this case a substantial part of the initial distribution has $m_p v_x^2/2 < e\phi_{\rm NIF}$, and one can expect to see a significant fraction of reflected ions. These are indeed clearly seen in Figure 4, right panel. In this case $T_u/m_p V_u^2 = 1/7$, $T_{d,\parallel}/m_p V_u^2 \approx 0.17$, and $T_{d,\perp}/m_p V_u^2 \approx 0.44$. Note that we always normalize the temperature on $m_p V_u^2$, where m_p is the proton mass.

Figure 5 shows the upstream (left panel) and downstream (right panel) distribution of the initially Maxwellian distributed singly ionized helium ions (HM). For these ions, v_T/V_u is twice as small while $mv_x^2/2$ is four times as large as the same parameters for protons, which means much weaker ion reflection. Indeed, the downstream distribution shows no population of reflected ions. The upstream and the downstream parallel temperatures are the same as for the protons. The downstream perpendicular temperature is due to the gyration of the ions, therefore, a significant fraction of the initial ion energy is converted into the perpendicular temperature, $T_{d,\perp}/m_p V_u^2 \approx 0.58$. This perpendicular temperature is much higher than that of the Maxwellian protons.

Figure 6 shows the upstream (left panel) and downstream (right panel) distribution of the initially VS distributed singly ionized helium ions (HV). The contribution of the reflected ions is substantially smaller than for VS protons since the electric reflection requires approximately

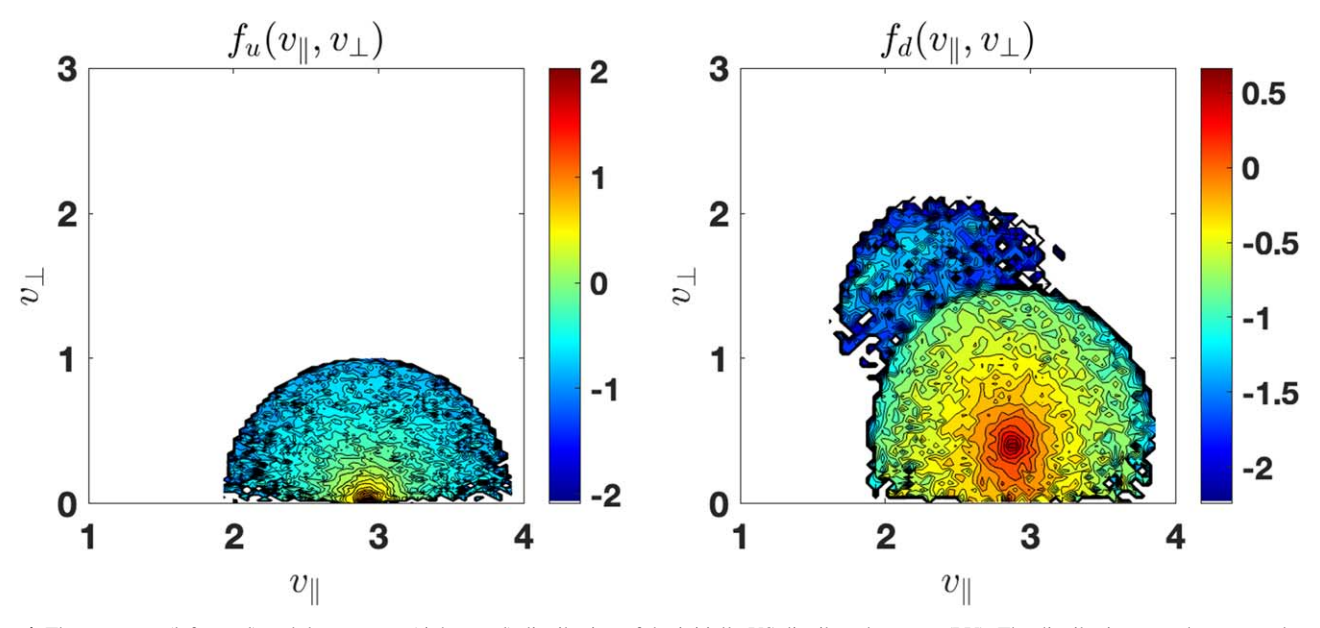


Figure 4. The upstream (left panel) and downstream (right panel) distribution of the initially VS distributed protons (PV). The distributions are shown on a log scale.

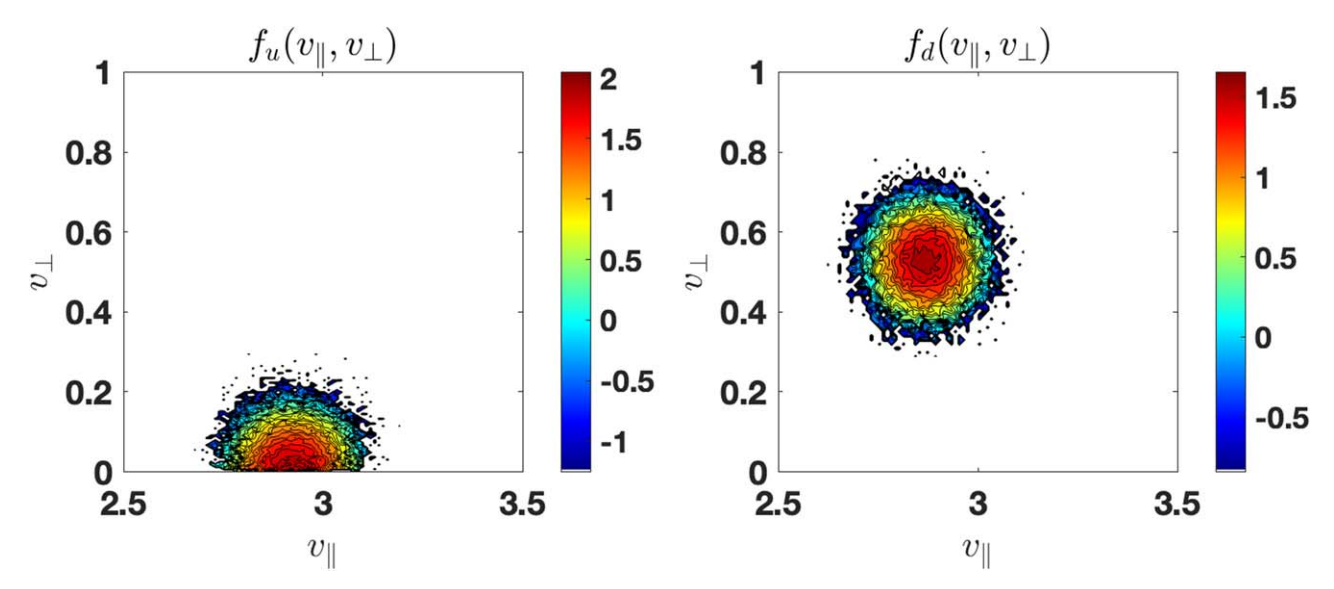


Figure 5. The upstream (left panel) and downstream (right panel) distribution of the initially Maxwellian He (HM). The distributions are shown on a log scale.

 $v_x^2/2 < e\phi_{\rm NIF}/m_{{
m He^+}} = e\phi_{
m NIF}/4m_p$. In this case

$$\frac{T_u}{m_p V_u^2} = \frac{4}{7}, \quad \frac{T_{d,\parallel}}{m_p V_u^2} \approx 0.62, \quad \frac{T_{d,\perp}}{m_p V_u^2} \approx 1.48.$$
(24)

Figure 7 shows the upstream (left panel) and downstream (right panel) distribution of the initially Maxwellian distributed α -particles (AM). In this case there is no parallel heating and $T_{d,\perp}/m_p V_u^2 \approx 0.52$.

Figure 8 shows the upstream (left panel) and downstream (right panel) distribution of the initially VS distributed α -particles (AH). In this case,

$$\frac{T_{d,\parallel}}{m_p V_u^2} \approx 0.63, \quad \frac{T_{d,\perp}}{m_p V_u^2} \approx 1.6.$$
 (25)

The contribution of reflected ions is larger for α particles than for singly ionized helium since $(m/q)_{\text{He}^+} = 2(m/q)_{\alpha}$.

The heating characteristics are summarized in Table 1. The most informative parameter is $\eta_{\rm species} = T_d / m_{\rm species} V_u^2$. There is

no reflection of thermal ions so that all the heating is due to the gyration of the directly transmitted ions (Gedalin 2021). The cross-shock potential reduces the normal component of the velocity upon crossing the shock:

$$v_{d,x}^2 = v_{u,x}^2 - 2\frac{q_{\text{species}}}{m_{\text{species}}}\phi.$$
 (26)

The temperature is then determined by $|v_{d,x} - v_{\text{drift}}|^2$, where v_{drift} is the downstream drift velocity along the shock normal. This drift velocity depends only on the magnetic compression and shock angle. For low upstream temperatures, $v_{u,x} \approx V_u$, so that the species with smaller q/m retain a large fraction of their initial energy and should be heated more strongly (Gedalin 2020). Accordingly, the downstream temperature of initially thermal He⁺ is higher than that for α particles, while protons have the lowest temperature, that is, $\eta_{p,M} < \eta_{\alpha,M} < \eta_{\text{He}^+,M}$. For superthermal upstream distributions, reflected particles make

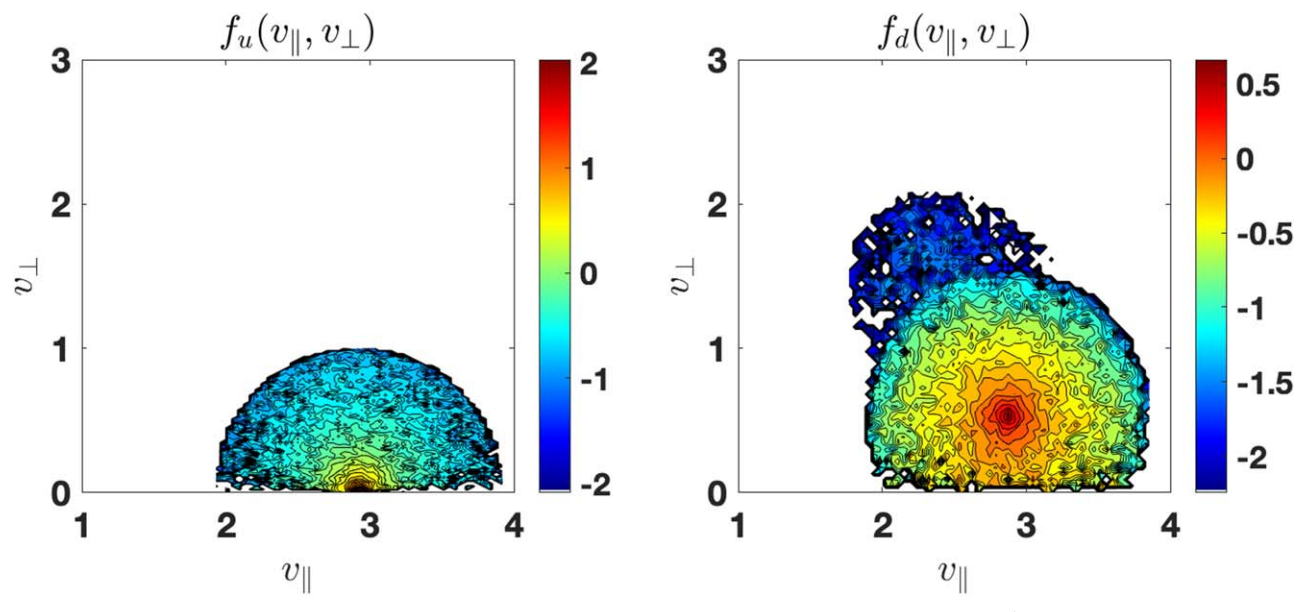


Figure 6. The upstream (left panel) and downstream (right panel) distribution of the initially VS distributed singly ionized He⁺ (HV). The distributions are shown on a log scale.

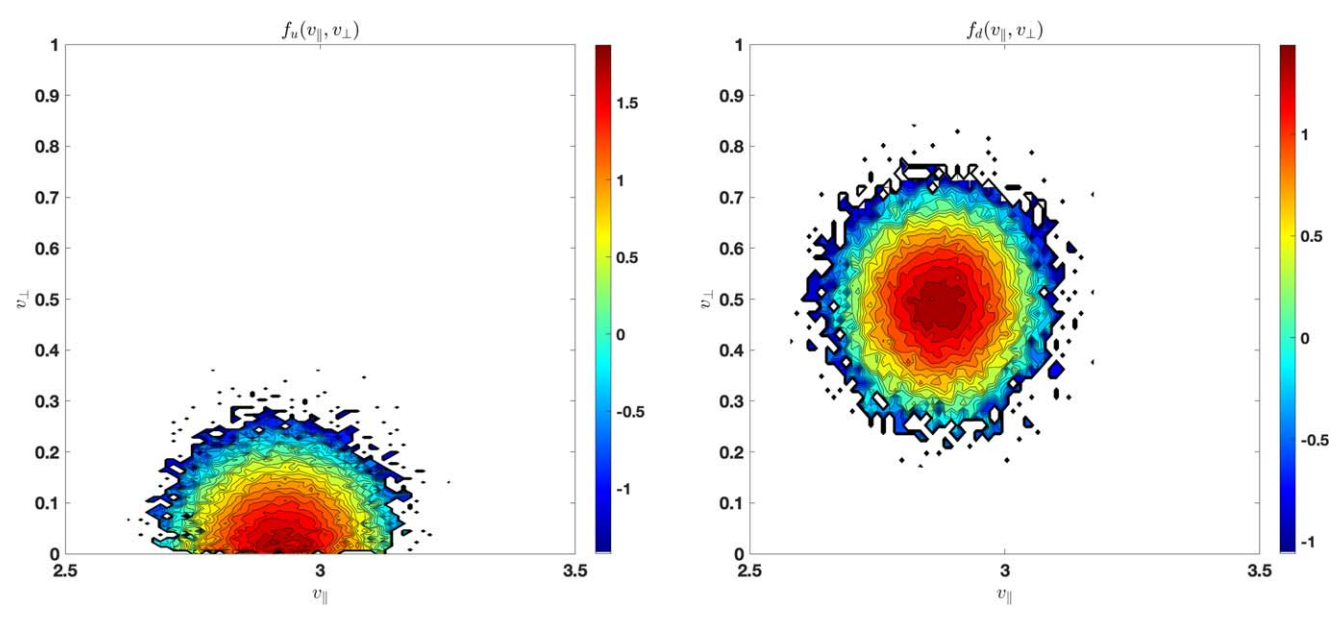


Figure 7. The upstream (left panel) and downstream (right panel) distribution of the initially Maxwellian α -particles (AM). The distributions are shown on a log scale.

the difference. Most of the ions are reflected due to the cross-shock potential. The effect of the cross-shock potential decreases with the decrease of q/m. The fraction of reflected protons is larger than the fraction of reflected α particles, while the fraction of reflected He⁺ is the smallest. Thus, $\eta_{p,\rm VS} > \eta_{\alpha,\rm VS} > \eta_{\rm He^+,\rm VS}$. Thermal ions are not heated in parallel direction, while for superthermal ions the parallel heating is weak but nonnegligible. For thermal ions, T_d/T_u is larger for larger m/q (Gedalin 2020). For superthermal VS ions, the ratio T_d/T_u decreases with the increase of m/q. In particular, this means that the relative heating of the pickup single-charged helium is almost two times smaller than the relative heating of the pickup protons.

4. Self-consistent Simulation

The analysis presented in the previous sections requires assumptions regarding the profile of the magnetic field and the magnitude and the structure of the shock potential. We next turn to a simulation that evolves simultaneously and self-consistently both particles and fields and demonstrate that the conclusions reached using particle-tracing calculations hold. We use a two-dimensional hybrid simulation that treats ion species in a fully kinetic manner and assumes that electrons are a massless fluid with a prescribed equation of state (see, e.g., Winske et al. 2003, for a general description of the hybrid method). The simulations were performed using the H3D code

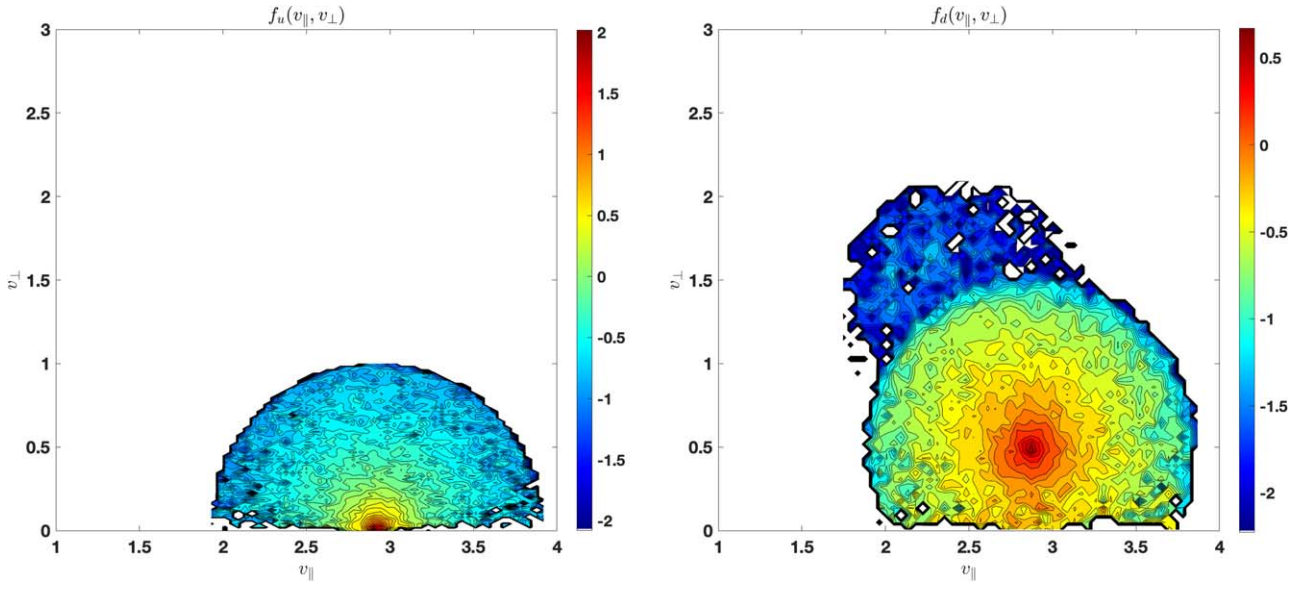


Figure 8. The upstream (left panel) and downstream (right panel) distribution of the initially VS distributed α particles (AV). The distributions are shown on a log scale.

	Table 1		
Downstream	Temperatures	and	Ratios

Parameter	Maxwell Protons	VS Protons	Maxwell He ⁺	VS He ⁺	Maxwell α	VS α
$\frac{T_{d,\perp}}{m_p V_u^2}$	0.11	0.44	0.6	1.48	0.52	1.6
$\frac{T_{d,\perp}}{mV_u^2}$	0.11	0.44	0.15	0.37	0.13	0.4
$\frac{T_{d,\perp}}{T_{u}}$	7.5	3.1	39.4	2.59	23.3	2.8
$\frac{T_{d,\perp}}{T_{d,\parallel}}$	7.5	2.62	39.4	2.4	23.3	2.54

(Karimabadi et al. 2006). The shock was initialized by reflecting plasma flow from a rigid wall. In addition to electrons with upstream density n_u and temperature T_u , the upstream plasma consisted of four populations of ions: (1) a dense proton core with density $n_1 = 0.97n_u$ and temperature T_u , (2) a superthermal population of protons with density $n_2 = 0.01n_u$ and a VS distribution, (3) a population of He⁺ with density $n_3 = 0.01n_u$ with Maxwellian distribution of temperature T_u , and (4) a superthermal population of He⁺ with density $n_4 = 0.01n_u$ and the VS distribution. The upstream speed of all populations, $V_u = Mv_A$, was the same and corresponded to $M \approx 2.6$ in the frame of the shock. The cutoff speed for all VS distributions was $u_c = V_u$. The magnetic field was oriented at an angle of $\theta_{\rm Bn} = 70^{\circ}$ with respect to the shock normal, and its strength B_u was chosen such that $\beta_u = 8\pi n_u T_u/B_u^2 = 0.1$. The simulation discussed here was performed in a domain of size $L_x \times L_y = (1024 \times 256)d_i$, $d_i = (c/\omega_p)$, with the resolution of $n_x \times n_y = (4096 \times 512)$ cells. The time step was $\delta t \Omega_u = 2.5 \times 10^{-3}$. Simulations with increased resolution and decreased time step were also performed to confirm the convergence of the presented results with respect to these parameters. A reference simulation with only the core Maxwellian protons was also performed.

Figure 9 illustrates the principal result of this study by showing the average profiles of the magnetic field and the parallel and perpendicular temperatures for all ion species. At the concentrations considered, ion populations other than Maxwellian protons have a relatively small impact on the overall structure of the shock, including the profile of the

magnetic field. In agreement with the predictions obtained using particle-tracing analysis, the increase in the perpendicular temperature is higher for Maxwellian distributions than for VS distributions, with He^+ experiencing the highest increase in T_{\perp} . The trend is reversed for VS distributions, with protons exhibiting larger heating than He⁺. The behavior of the He⁺ population with Maxwellian upstream distribution is notable in that, in contrast to other populations, it is transmitted through the shock like a beam and takes a considerable distance (more than a $100d_i$) to become gyrotropic downstream. One manifestation of this is the appearance of large periodic fluctuations in T_{\perp} for this population. The same signatures are also present but are much weaker in the VS He⁺ populations. The proton populations become gyrotropic on much smaller scales. None of the populations become isotropic on the scales considered.

5. Conclusions

In a planar, stationary low-Mach number shock, ion heating occurs in the direction perpendicular to the magnetic field. Parallel heating is weak and even negligible. Anisotropy of the ion distributions behind the shock transition should be removed or reduced by other processes, not included in the present analysis. Heating of protons and heavier ions is different because of the different mass-to-charge ratio. The larger the ratio, the weaker the ion reflection for the same shock angle, magnetic compression, and cross-shock potential. Accordingly, the downstream perpendicular temperature per mass is smaller

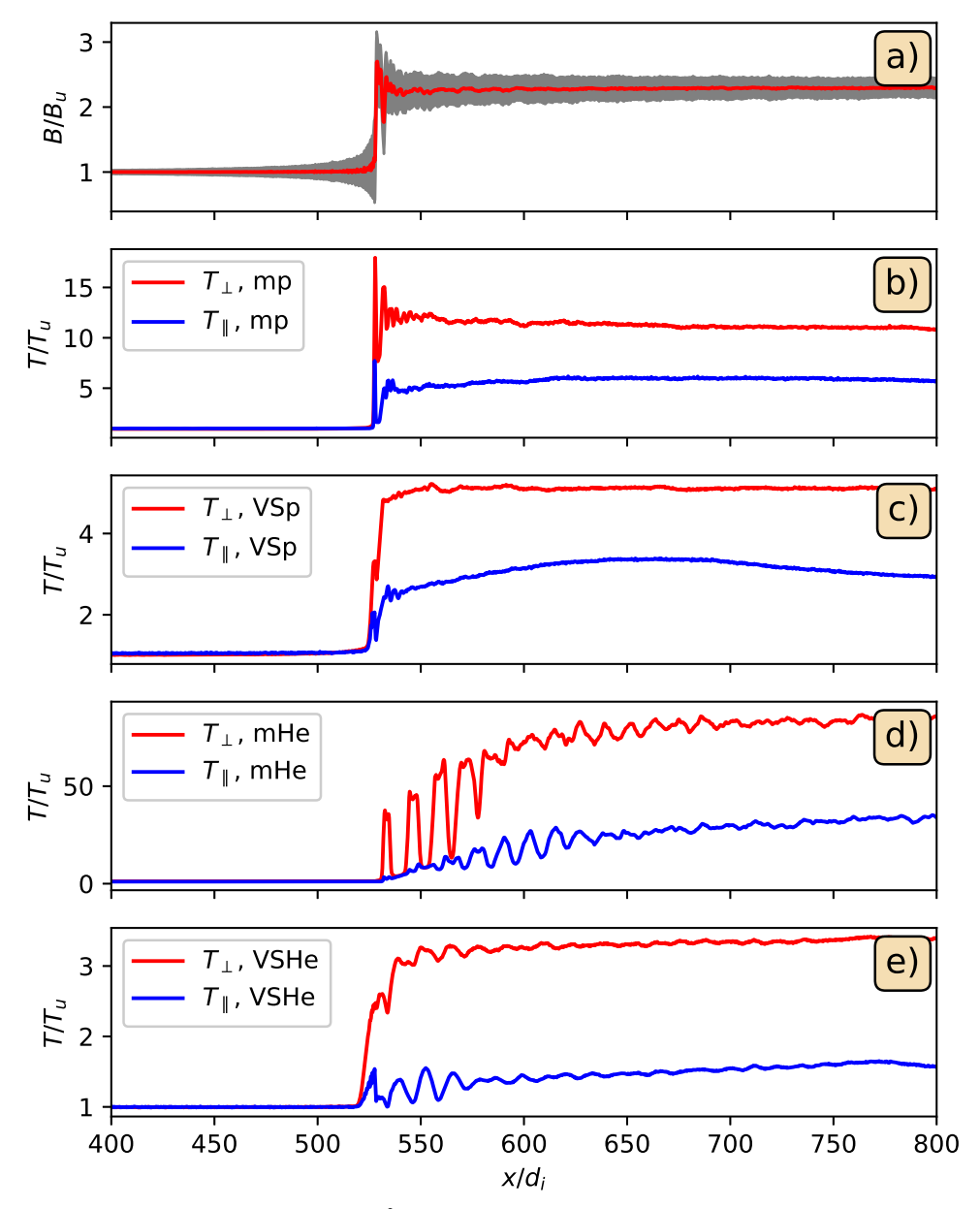


Figure 9. Hybrid simulation of a shock with $M_A \approx 2.6$ and $\theta_{\rm Bn} = 70^{\circ}$ in a multicomponent plasma: (a) profile of the average magnetic field (solid red line) and the amplitude of the magnetic fluctuations (shaded area representing \pm standard deviation from the mean); (b)–(e) profiles of the average perpendicular and the parallel temperatures (with respect to the local magnetic field) for Maxwellian protons (mp), VS protons (VSp), Maxwellian He⁺ (mHe), and VS He⁺ (VSHe), respectively. The averages are taken over y-direction at a fixed x.

for larger m/q. For low-temperature upstream Maxwellian distributions, there are no reflected heavy ions at all since reflected ions come from the tail of the distribution roughly satisfying the requirement $mv_x^2/2 < 2q\phi_{\rm NIF}$. Heating of superthermal distributions differs from the heating of thermal Maxwellian ions. VS distributions represent a class of strong superthermal distributions without particles moving away from the shock in the upstream region. Ion reflection is much stronger in superthermal distributions since the fraction of ions satisfying the reflection condition is much larger. The usage of VS allowed us to clearly separate thermal ions from superthermal ones. No backstreaming ions are produced for the

shock angle used in this study. This issue was treated by Gedalin et al. (2021).

M.G. was partially supported by NSF-BSF grant 2019744 and by the European Union's Horizon 2020 research and innovation program under grant agreement No 101004131 (SHARP). N.P. was supported, in part, by NSF-BSF award 2010450 and NASA grant 80NSSC18K1649. N.P. was additionally supported by the IBEX mission as a part of NASA's Explorer program. V.R. was partially supported by NASA grant 80NSSC18K1649 and NSF-BSF award 2010144. Resources supporting this work were provided by the NASA

High-End Computing (HEC) Program through the NASA Advanced Supercomputing (NAS) Division at Ames Research Center.

ORCID iDs

Michael Gedalin https://orcid.org/0000-0003-1236-4787 Vadim Roytershteyn https://orcid.org/0000-0003-1745-7587 Nikolai V. Pogorelov https://orcid.org/0000-0002-6409-2392

References

```
Abraham-Shrauner, B. 1967, JPIPh, 1, 379
Bale, S. D., Bale, S., Mozer, F. S., et al. 2003, PhRvL, 91, 265004
Bale, S. D., Balikhin, M. A., Horbury, T. S., et al. 2005, SSRv, 118, 161
Balikhin, M., & Gedalin, M. 2022, ApJ, 925, 90
Broll, J. M., Fuselier, S. A., Trattner, K. J., et al. 2018, GeoRL, 45, 49
Burgess, D., Wilkinson, W. P., & Schwartz, S. J. 1989, JGR, 94, 8783
Gedalin, M. 1996, JGR, 101, 4871
Gedalin, M. 1997a, GeoRL, 24, 2511
Gedalin, M. 1997b, SGeo, 18, 541
Gedalin, M. 2016, JGR, 121, 10,754
Gedalin, M. 2020, ApJ, 900, 171
Gedalin, M. 2021, ApJ, 912, 82
Gedalin, M., Dröge, W., & Kartavykh, Y. Y. 2015, ApJ, 807, 126
Gedalin, M., Pogorelov, N. V., & Roytershteyn, V. 2021, ApJ, 910, 107
Génot, V. 2009, ASTRA, 5, 31
Greenstadt, E. W., Russell, C. T., Scarf, F. L., Formisano, V., &
   Neugebauer, M. 1975, JGR, 80, 502
```

```
Hobara, Y., Balikhin, M., Krasnoselskikh, V., Gedalin, M., & Yamagishi, H.
  2010, JGR, 115, 11106
Hudson, P. D. 1970, P&SS, 18, 1611
Karimabadi, H., Vu, H., Krauss-Varban, D., & Omelchenko, Y. 2006, in ASP
   Conf. Ser. 359, Numerical Modeling of Space Plasma Flows, ed. G. Zank &
   N. Pogorelov (San Francisco, CA: Astronomical Society of the Pacific), 257
Karimabadi, H., Vu, H., Krauss-Varban, D., & Omelchenko, Y. 1988, JGR,
Krasnoselskikh, V., Balikhin, M., Walker, S. N., et al. 2013, SSRv, 178, 535
Leroy, M. M., Winske, D., Goodrich, C. C., Wu, C. S., & Papadopoulos, K.
  1982, JGR, 87, 5081
Lynn, Y. M. 1967, PhFl, 10, 2278
Mellott, M. M., & Greenstadt, E. W. 1984, JGR, 89, 2151
Newbury, J. A., Russell, C. T., & Gedalin, M. 1998, JGR, 103, 29581
Pope, S. A., Gedalin, M., & Balikhin, M. A. 2019, JGR, 165, 3
Richardson, J. D. 2010, GeoRL, 37, 12105
Russell, C. T., Hoppe, M. M., Livesey, W. A., Gosling, J. T., & Bame, S. J.
  1982, GeoRL, 9, 1171
Sckopke, N., Paschmann, G., Bame, S. J., Gosling, J. T., & Russell, C. T. 1983,
   JGR, 88, 6121
Sckopke, N., Paschmann, G., Brinca, A. L., Carlson, C. W., & Luhr, H. 1990,
  JGR, 95, 6337
Scudder, J. D., Mangeney, A., Lacombe, C., et al. 1986, JGR, 91, 11019
Vasyliunas, V. M., & Siscoe, G. L. 1976, JGR, 81, 1247
Vogl, D. F., Biernat, H. K., Erkaev, N. V., Farrugia, C. J., & Mühlbachler, S.
   2001, NPGeo, 8, 167
Winske, D., Yin, L., Omidi, N., Karimabadi, H., & Quest, K. 2003, in Space
  Plasma Simulation, Vol. 615, ed. J. Büchner, M. Scholer, & C. T. Dum
  (Berlin: Springer), 136
Woods, L. C. 1971, PlPh, 13, 289
Woods, L. C. 1969, JPlPh, 3, 435
Zimbardo, G. 2011, P&SS, 59, 468
```

Greensadt, E. W., Russell, C. T., Gosling, J. T., et al. 1980, JGR, 85, 2124